JOURNAL OF PROPULSION AND POWER
Vol. 25, No. 1, January–February 2009

Aerothermal Analysis of a Partially Shrouded Axial Turbine

L. Porreca,* A. I. Kalfas,† and R. S. Abhari‡
Swiss Federal Institute of Technology (ETH), 8023 Zürich, Switzerland

DOI: 10.2514/1.34902

This work presents the results of the aerodynamic and thermostructural analysis of three different shrouded axial turbine configurations. The blade geometry of the turbine stages and the tip clearances of the test cases under investigation are identical although the shroud design is varied. The first test case is representative of a full shroud geometry, and the second and third test cases adopt different partial shroud arrangements. The aerodynamic characteristics of these geometries have been investigated in previous studies, which are summarized in this paper. The influence of the shroud geometry on the heat load and mechanical stresses has been evaluated by a conjugate heat transfer approach coupled with finite element analysis. The combination of aerodynamic, centrifugal, and thermal loads has been applied to the solid blade model. Results show that the full shroud test case has higher mechanical stresses on the blade root but lower stress concentrations on the blade/shroud components. The partial shrouded cases have the lowest blade root stress. The last geometry is an optimized partially shrouded design, showing an improved lifetime achieved by a better stress distribution over the blade shroud compared to the other two cases. The effect of the shroud configuration on the aerodynamic performance, heat load, and mechanical stresses has been summarized, quantified, and discussed in detail. The combination of aerodynamic measurements and computational analysis shows that an optimum between aerodynamic performance and blade life is achieved by applying a small modification to the partial shroud geometry.

Nomenclature

h	=	heat transfer coefficient
k	=	thermal conductivity
L	=	characteristic length
Ma	=	Mach number
Nu	=	Nusselt number
Pr	=	Prandtl number
Ps	=	static pressure
Pt	=	total pressure
$\dot{q}$	=	heat flux
Re	=	Reynolds number
T	=	temperature
t	=	rupture time, h
α	=	yaw angle
β	=	pitch angle

Subscripts

wall	=	wall temperature
ref	=	mass-averaged total temperature

INTRODUCTION

THE sealing between moving blade row and stationary components in turbomachinery such as the casing is achieved with using a shrouded or unshrouded design of the tip blade. The leakage flow from the tip is still considered as a main source of aerodynamic losses. Obviously, the smaller the gap, the lower the losses. However, mechanical and thermal tolerances do not allow the reduction of this gap to less than, typically, 1% of the blade height. Minimizing the aerodynamic losses and maintaining tight tip clearances over the life of the engine in such a high temperature environment is still a critical issue in modern turbomachinery design.

Shrouding turbine blades ensures more effectively sealing this gap, leading to an increase of aerodynamic efficiency. However, this design requires a more complex cooling arrangement to ensure reasonable temperatures in the shroud itself. The cooling arrangement significantly increases the manufacturing cost per blade. Additionally, the increased weight at the highest radius of the blade considerably increases the blade/disk centrifugal stresses. For these reasons, a number of alternative solutions are under consideration such as partial shrouds or winglets. Previous investigations focused on the aerodynamic behavior of these devices as found by Yaras and Sjolander in [1], Harvey et al. [2], Harvey and Ramsden [3], Nirmalan and Bailey [4], Schabowski and Hodson [5], and Porreca et al. [6].

Although a large number of papers have been published on unshrouded blades, shrouded geometries have generally received less attention regarding the heat transfer issue due to their difficult use on the harsh environment of the HP turbines. There are, however, a number of manufacturers that successfully use shrouded blades in the HP turbine section. With respect to the unshrouded blade, some differences should be noted. The leakage flow that originates from the outer part of the flow exiting the upstream nozzle guide vane (NGV) usually has a lower temperature with respect to the main stream. This relatively "cold" stream enhances the shroud cooling which is heat loaded only from the underside. Additionally, shrouds are large enough to include an internal cooling system with ejection holes on the shroud surface. An example of such an arrangement can be found by Evans et al. in [7], Dorris et al. [8], and Tomita [9]. Obviously cooling the shroud requires an additional mass flow extraction from the compressor section and therefore a penalty in the overall thermodynamic cycle efficiency. According to Harvey [10], this amount of coolant flow is not considered as prohibitive in the current application of such a shroud in a modern turbofan engine. However, no quantification of the amount of this coolant flow is available in the open literature. Nirmalan et al. [11] performed an

Presented as Paper 1299 at the ISABE 2007 18th International Symposium on Airbreathing Engines, Beijing, China, 2–7 September 2007; received 1 October 2007; revision received 4 August 2008; accepted for publication 6 August 2008. Copyright © 2008 by the American Institute of Aeronautics and Astronautics, Inc. All rights reserved. Copies of this paper may be made for personal or internal use, on condition that the copier pay the $10.00 per-copy fee to the Copyright Clearance Center, Inc., 222 Rosewood Drive, Danvers, MA 01923; include the code 0748-4658/09 $10.00 in correspondence with the CCC.

*Ph.D., Research Engineer, LEC—Laboratory for Energy Conversion; current address: MAN Turbo AG Schweiz, Zurich, Switzerland; luca.porreca@man.eu.

†Senior Scientist, LEC—Laboratory for Energy Conversion; current address: Aristotle University of Thessaloniki, Thessaloniki, Greece. Member AIAA.

‡Professor, Head of the Department, LEC—Laboratory for Energy Conversion.

experimental and numerical investigation on the heat transfer effectiveness around the shroud in a cooled linear cascade with the same "scalloped" geometry reported by Nirmalan and Bailey [4]. Coolant flow was varied between 0.75 and 1.12% of the passage flow.

More recently, due to heightened pollution regulation for gas turbine systems (especially NOx), the combustion chamber uses more air in the primary zone. This affects the temperature profile at the inlet of the first HP stage, and the result of this lean combustion process is a significant increase of the heat load on the hub and tip endwall. For this reason, a more efficient shroud cooling is required and several strategies are currently under investigation. Kanjirakkad et al. [12] and Janke et al. [13] recently published an experimental and numerical study on the passive shroud cooling concepts.

This study presents an aerothermal comparison of three test cases with the same blade geometry but different shroud representative of a full shroud (FS) configuration, partial shroud (PS), and a modified partial shroud geometry (EPS). The overall effect of the partial shroud geometry on the turbine aerodynamic is an increase of flow unsteadiness, which significantly affects the flowfield in both rotating and stationary blade rows. A significant change in the aerodynamic efficiency has been measured in the second stage. The effect of the shroud geometry on the heat transfer is an overall reduction of the total heat transferred on the shroud surface. However, higher temperature gradients are observed in the partial shroud cases that result, in the PS test case, in a higher thermal stress concentration. The EPS test case presents the lower mechanical stresses that result in a longer lifetime estimation.

Turbine Configurations

The test cases under investigation are representative of a modern gas turbine blading used for power generation purposes. The aerodynamic design of the two stages includes noncylindrical stacking of both stator and rotor and smooth geometry downstream of the rotor shroud. Three test cases are taken into consideration in this work. The airfoil geometry is the same in all test cases except the design of the shroud on both rotors 1 and 2. (shown in Fig. 1). The first test case (named FS in the following sections) uses a full axis-symmetric shroud typical of modern engine designs that is adapted to the geometrical constraints of the parallel annulus of the facility. This shroud has three inclined forward fins and a one-step labyrinth path in the first rotor and a two-step path in the second rotor. The other two test cases use partial shroud arrangements. The PS case has two vertical fins with a one-step labyrinth path and a nonaxisymmetric shroud platform and cutback at the leading and trailing edges (TE). Moreover, the shroud platform leaves the region from about 65% Cax (axial chord) to the blade TE uncovered.

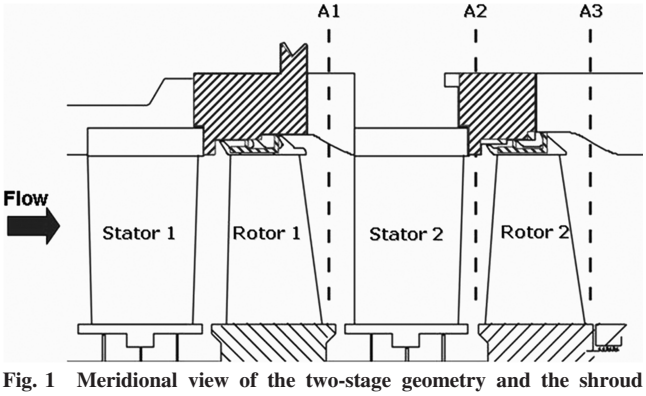

Fig. 1 Meridional view of the two-stage geometry and the shroud different configurations.

The EPS has a similar geometry to the PS case but the shroud platform partially covers the blade passage at the trailing edge as shown in Fig. 2. The tip clearance is constant for all cases and equal to 1% of the blade height. All test cases are examined at a constant turbine pressure drop and constant rotational speed. The mass flow is then a result of the slightly different flow capacity due to the different shroud geometry.

Experimental Setup

The experimental investigation was performed on the research turbine LISA at the Turbomachinery Laboratory of the ETH Zurich. The facility can accommodate up to two stages of an axial turbine. The air loop is a closed type and includes a radial compressor, a two-stage water-to-air heat exchanger, and a calibrated venturi nozzle for accurate mass flow measurements. A generator absorbs the turbine power and controls the rotational speed of the turbine shaft. The first and the second rotors are mechanically decoupled by a twin spool shaft design. The torque of each of the two stages is measured by independent torquemeters. To achieve the same rotational speed, both shafts are coupled again before the generator. A sketch of the turbine section is presented in Fig. 1. More details can be found in [14].

The turbine design allows quick and precise assembly and easy access to the measurement planes. A number of different intrusive (probes) and nonintrusive measurement (particle image velocimetry) techniques are applied. The facility is equipped with a 4-axis numerically controlled positioning system with ultrahigh precision in each direction. The turbine is typically operated at a constant pressure drop across the stages. The turbine inlet temperature is controlled with an accuracy of 0.3% and the rotational speed is kept constant by the dc generator with a range of $\pm 0.02\%$ (± 0.5 rpm). The main operational parameters of the facility are listed in Table 1.

Steady-state measurements are performed using miniaturized pneumatic five-hole probes (5HP) with a 0.9-mm-diam cobra head shape (Treiber et al. [15]). The probe is calibrated for ranges of ± 14 deg in yaw and ± 30 deg in pitch angle. The uncertainties of pneumatic 5HP probe measurements for angles of ± 10 deg in yaw and ± 10 deg in pitch are as follows: $\alpha = 0.3$ deg, $\beta = 0.3$ deg, $Pt = 60$ Pa, $Ps = 130$ Pa, and For larger pitch angles, the uncertainty is higher.

The measurement grid comprises 1502 points that are distributed uniformly in the circumferential direction at every 3.5% pitch (32 points in a pitch range of 1.1) and 47 points clustered toward the endwalls in the radial direction.

Numerical Method

The full stator and rotor passage for both stages are modeled in the computational mesh using the commercial software CENTAUR,

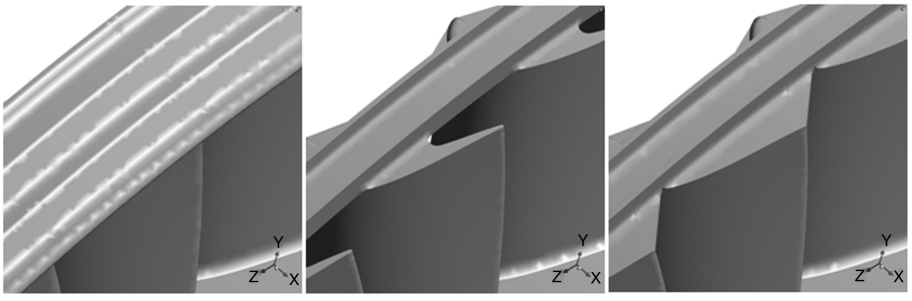

Fig. 2 Schematic of the shroud geometry: FS (left), PS (middle), and EPS (right).

Table 1 Main parameter of LISA 2-stage axial turbine research facility

Rotor speed, rpm	2625
Overall pressure ratio	1.38
Mass flow, kg/s	10.65
Blade count (stator/rotor)	42/42
Aspect ratio	1.8
Mach number (stator/rotor)	0.35/0.1
Reynolds number (rotor)	2×10^5

excluding only the labyrinth path at the hub region. The tip clearance and shroud geometry are fully modeled in the meshing process (Porreca et al. [6]). To facilitate efficient meshing of the nonaxisymmetric partial shroud geometry and to reduce the turn around time for grid generation, unstructured meshes covering both the main flow path and the tip leakage paths were chosen for all the test cases. Because of the same blade count number in both stator and rotor passages, the computational domain is limited to only one blade passage. Periodic boundary conditions are applied.

The total number of elements for both stages is about 2.7×10^6 corresponding to 1.2×10^6 nodes. The stator mesh is limited to 1.7×10^5 nodes while the rotor blades, due to the resolved labyrinth seal passage, accounts for about 4×10^5 nodes. The resulting averaged nondimensional wall distance for all test cases is between 6.5 and 9.9 in the shroud region and to 25 on the rotor blades.

The simulations were performed using the commercial flow solver Ansys CFX 10.0, which is an element-based conservative finite-volume method. All the calculations started with a frozen rotor (i.e., no averaging at the interface stator/rotor). Then the solution was switched using a mixing plane method in which all the flow quantities are averaged in the circumferential direction at the stator/rotor interface. The solution residuals were monitored continuously for the momentum, energy, and turbulence equations. The residuals in all cases drop from $10e-2$ to $10e-6$ for the momentum equations, while the energy equation residual drops to $10e-5$.

The measured total pressure, total temperature, and flow angle distributions at the inlet were prescribed to the computational domain. The flow was assumed to be fully turbulent and turbulence closure was achieved using a standard k–ε turbulence model. The inlet turbulence intensity of 2% and a turbulent length scale of 0.1 m have been chosen to reflect the flow conditions of the test facility. A reference static pressure at the hub exit and the radial equilibrium condition were prescribed at the outlet. All walls were assumed to be adiabatic to reproduce the thermal equilibrium conditions achieved during the experiments and validate the numerical approach with the measurements.

To simulate the influence of the shroud geometry on the heat load and the mechanical stresses, the numerical simulations were also done under engine representative conditions. The operation point of the test cases is scaled to high temperature conditions by means of a nondimensional similitude analysis. In particular, the pressure ratio and the corrected rpm are kept constant in both the cold case (representative of the current experimental conditions) and the "hot" case (engine conditions). Once these inlet conditions are defined, by keeping the above nondimensional parameters constant, the turbine operation point can be scaled guaranteeing the design flow velocity triangle. The level of inlet turbulence intensity and turbulent length scale were kept the same as in the cold case. The boundary conditions for the hot case are as follows:

$$P_{01} = 8 \times 10^5 \text{ Pa} \qquad T_{01} = 1470 \text{ K}$$

$$P_{01}/P_3 = 1.38 \qquad \text{rpm} = 5643$$

Details and validation of the numerical solution against experimental data can be found in Porreca et al. [6].

Conjugate Heat Transfer Analysis

The aim of the simulation in engine representative conditions is to evaluate the temperature distribution on the solid blade to assess the metal thermal gradient. For this reason a conjugate heat transfer (CHT) methodology has been applied. This approach allows the simultaneous solution of the external fluid dynamics and conduction problem within the solid and has been successfully applied by several authors such as Bohn et al. [16], Moser et al. [17], and Takahashi and Watanabe [18].

A solid model of the blade is created for the first and second rotors. The stator blade rows are considered as adiabatic. To guarantee a full overlap between the fluid and the solid domain, three fluid passages are modeled for each solid blade. The solid grid is of the unstructured type and has about 1.3×10^5 nodes. To take into account a realistic blade environment in the hot case calculation, an internal cooling channel has been designed for both the first and second rotors. Therefore, the blade temperature distribution is the result of a combination of heat flux from the fluid, thermal conductivity of the metal and internal convection from the cooling passage. The design of the cooling channel has been made by reproducing a three-passage duct with a flow ejection from the TE. Figure 3 shows a circumferential cut at midspan of the fluid and solid domain and the internal cooling passage. The coolant flow ejection from the blade trailing edge has not been considered in the present model. On the surface of the cooling passage a heat transfer coefficient and a inlet flow temperature have been set as boundary conditions.

The selection of these parameters has been made by using data from the open literature. The coolant fluid is often taken from the outlet of the compressor section. For a gas turbine plant of about 200 MW and a compression ratio of 32:1, the exit temperature is about 743 K. The heat transfer coefficient has been retrieved form experimental data of advanced cooling strategies in rotating channel geometry.

Several studies focused on the enhancement of the heat transfer coefficient in cooling channels. Commonly, a variety of different geometries are used to increase the turbulence and therefore the convection heat transfer coefficient. Wright et al. [19] and Griffith et al. [20] compared different dimpled, angled, and discrete angled V-shaped and W-shaped ribs in the channel. They found that superior overall performances are achieved by the discrete V- and W-shaped ribs in rotating and nonrotating channels. The comparison is done with reference to the Dittus-Boelter/McAdams Nusselt number correlation (Nu_0) for a fully developed turbulent flow through a smooth stationary circular tube:

$$Nu_0 = 0.023 Re^{0.8} Pr^{0.4}$$

In the present analysis, a Reynolds number of 4×10^4 has been considered and a value of Nusselt ratio Nu/Nu_0 equal to 3 has been selected as a mean value between the different rib configurations (Wright et al. [19]). In the cooling channel geometry taken into account in the present study, the corresponding heat transfer coefficient is equal to 1600 $\text{W/m}^2\text{K}$.

In addition to the internal convection cooling, shrouded HP turbine blades also require cooling in the tip section where the shroud is located. Normally, the cooling of this component is done with internal cooling passages (active cooling) or impinging jets from the

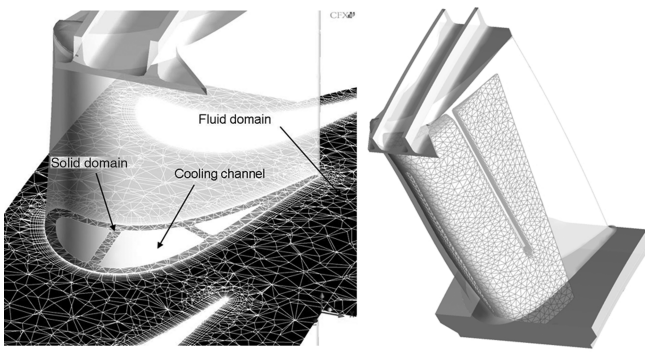

Fig. 3 Fluid/solid domain and internal cooling passage geometry.

stationary frame (passive cooling). In the present study a model of passive cooling is implemented in the CHT simulation.

A series of impinging jets are modeled in the first and second rotor stationary casing rings to provide the required cooling air to the upper surface of the shroud. The effect of the cooling in the shroud is modeled by introducing a source term in the boundary conditions of the energy equation on the nodes located on the shroud surface on the solid domain.

Cooling by means of impinging jets is commonly used in several engineering applications like electronic-chip cooling, paper and fabric drying, cooling of hot metal sheets, as well as rotating machinery. Han and Goldstein [21] published a review of the common impingement jet strategy used in gas turbine application. A heat transfer coefficient in impinging jets is usually presented as a function of the jet hole Reynolds number, the diameter D, the distance of the plate from the hole H/D, and the radial distance from the jet centerline r/D.

In this study a row of 20 impingement holes per pitch is considered with a diameter of 1 mm each. The coolant mass flow is set to 0.5% of the total mass flow evaluated in the engine representative conditions. The jet velocity corresponding to this configuration is equal to 50.7 m/s that corresponds to a Reynolds number of about 5×10^3. With a jet hole diameter of 1 mm, the distance H/D of the shroud surface is about 8 in the EPS and EPS test case and about 5 in the FS case. Therefore, an averaged value of Nusselt number equal to 15 was selected according to Brevet et al. [22] and Son et al. [23]; this corresponds to a heat transfer coefficient equal to 740 $\mathrm{W/m^2K}$.

The heat flux set as boundary conditions in the shroud surface can be thus written as

$$\dot{q}_{\text{cooling}} = h(T_{\text{metal}} - T_{\text{cooling}})$$

where h is the averaged impinging jet heat transfer coefficient evaluated above, T_{metal} is the averaged temperature of the shroud surface, and T_{cooling} is the bulk temperature of the jet. Because the metal temperature of the shroud surface is not known a priori, an iterative procedure must be done to be converged on the value of the heat flux. The procedure converged after 3–4 steps.

Finite Element Analysis

To quantify the effect of the shroud geometry on the blade mechanical stresses, a finite element analysis has been performed on the three test cases. In the solid model of the blade, three different loads have been applied, specifically: 1) a centrifugal load resulting from rotational speed, 2) an aerodynamic load, and 3) a thermal load. The root surface has been fixed on the frame of reference whereas the shroud side surfaces are left free to be deformed and displaced. A common practice in mechanical design and assembly is to profile the shroud periodic side surfaces to "interlock" the blades to each other. This design requires that, during the assembling of the rotor, the blades are slightly twisted and a stress is applied on the shroud boundaries. During operation, this stress is partially released due to the centrifugal stresses and thermal expansion. However, the interlock guarantees a higher stiffness and increased damping at the highest radius of the blades and thus a reduction of vibrations (Berruti et al. [24], Griffin [25], and Berthillier et al. [26]).

In some HP turbine designs, however, the shroud interlock induces a high stress concentration that results in material creep. Different approaches have been proposed to locally reduce the creeping deformation by introducing a reinforcing material in the shroud such as ceramic-matrix composites or reinforcing rods or bars into the casting of the shroud (Herron [27]). However, in some cases, this design is not applied and the blade is designed and certified by considering the blade as not attached to his neighbor, thus without the beneficial mechanical effect of the shroud interlock. In the present analysis, this practice is taken into account and therefore, in all test cases, the shroud side surfaces are free to deform, rotate, and displace in any direction due to the centrifugal load, pressure, and temperature field.

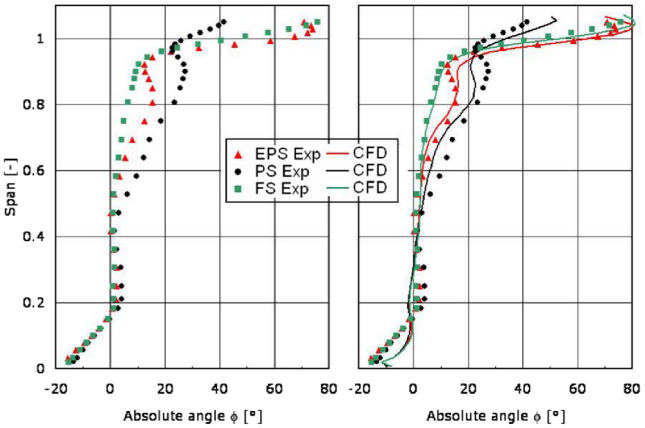

Fig. 4 Mass-averaged yaw angle at the turbine exit: plane A3—Exp data (left); Exp and CFD data (right), from Porreca et al. [6].

Effect of the Shroud on the Aerodynamic Performance

The effect of the shroud on the turbine flowfield is evaluated by means of aerodynamic measurements performed in the turbine facility LISA and reported in detail in [6]. Results indicate that the entire flowfield is dominated by the effect of the different shroud geometries. The uncoverage of the blade throat in the PS case causes the flow to expand in both the first and second rotors in the cavity region and reenter in the main path.

An optimized partial shroud geometry is used in the EPS case adopting a platform onto the trailing-edge region of the rotor blade to prevent the flow expansion in the cavity region. Figure 4 shows the absolute yaw angle measured downstream of the second rotor. The same flow features are similar up to midspan. A significant underturning occurs in the PS case, and the measured angles are about 20 deg different with respect to the reference FS test case. Moreover, the presence of underturning/overturning between 90 and 100% span shows the presence of the tip vortex that occurs in the PS case. Within the leakage layer (blade span greater than 100%), the PS case has only a moderate swirl which indicates that mixing between the leakage flow and the main stream has occurred upstream during the expansion of the main flow in the cavity region. The FS case on the other hand has a almost constant yaw angle up to 90% span and then, similar to the first rotor, the main flow tends to be aligned with the leakage layer. The yaw angle of the EPS case presents a profile that lies in between the FS and PS cases. The computational fluid dynamics (CFD) results (Fig. 4, right) are in good agreement with the measured absolute yaw angle. The main flow as well as the overturning/underturning is well captured with differences limited to ± 1 deg at midspan and ± 2 deg in the tip secondary flow region.

The second stage aerodynamic efficiency has been measured using a mechanical method. The FS test case with a full shroud arrangement has the highest efficiency of all the operating points. The PS test case has an aerodynamic efficiency penalty of about 1.1% at design conditions and between 0.8 and 1% at off-design conditions (Table 2). This penalty arises from the flow angle distribution along the radius in both rotors and the different flowfield at the blade tip. High deviations between measured and design flow angles are detected and a significant unloading from 60 to 100% span is observed. Moreover, a strong tip leakage develops due to the uncovering of the throat passage. Consequently, the mixing process

Table 2 Measured total-to-total second stage relative efficiency for the PS and EPS test cases: FS* reference case

Total-to-total efficiency 2nd stage, %			
Turbine pressure difference, Pa	FS*	PS	EPS
33,900	100	−1.0	——
37,485	100	−1.1	−0.5
40,575	100	−0.8	——

is enhanced and losses are generated. In the EPS test case the shroud is extended toward the trailing edge of the rotor blade and partially covers the blade passage. The formation of the tip vortex is reduced and flow angles are in between the FS and the PS cases. The blade loading control is also improved when compared to the PS case. The second stage efficiency is thus improved by 0.6%.

Effect of the Shroud on the Heat Load

Conjugate heat transfer analysis is used to quantify the effect of the shroud geometry on the blade heat load. Using the CHT approach, the heat transfer at the fluid and the solid interface is determined. For comparison purposes this parameter is presented in nondimensional form as a Nusselt number defined as

$$Nu = \frac{\dot{q}L}{k(T_{\text{ref}} - T_{\text{wall}})}$$

where the reference temperature has been set as the stage inlet mass-averaged total temperature. The Nusselt number distribution on the pressure and suction surfaces of the second rotor is shown in Fig. 5 at three blade span heights (15% midspan and 85% span) on the second rotor. On the abscissa the nondimensional blade axial chord is shown. A negative value indicates the blade pressure side whereas positive values indicate the suction side. At the hub, because the flow features are almost identical for all test cases, the Nusselt number is nearly unchanged. At midspan, even though the aerodynamic influence of the shroud geometry is very limited, the Nusselt number varies on both the pressure and the suction sides. The slightly different incidence resulting from the different evolution of the secondary flow on the second stator is the reason for this behavior. As expected, major differences on the heat load are found at the tip region at 85% span, due to the presence of different secondary flow structures. On the pressure side, the FS and the EPS cases have shown almost the same values because the flow incidence at this span is quite similar. However, the PS case has lower Nusselt numbers due to the negative flow incidence. On the suction surface, the FS and EPS show similar behavior upon an axial location of about 0.65. This location corresponds to the end of the second vertical fin in the partial shroud case. As described in the previous section, the passage vortex expands at this location. As a result of this expansion, the Nusselt number in the EPS and PS cases has a sudden reduction whereas in the FS case, where the flow is guided until the blade trailing edge, the Nusselt number is higher compared to the other cases. However, at a higher blade span, the effect of the vortex dynamics in the partial shroud cases is to increase substantially the convective heat transfer and therefore, the Nusselt number at the blade tip close to the trailing edge is about 1000 in the PS and EPS cases, while in the FS case, the trailing edge has much lower values across the whole span. In the PS case, at the blade tip corresponding to the blade suction side, an increase of the Nusselt number is observed up to 1500. This behavior has an effect on the temperature distribution on the blade tip surface. The total heat transferred from the flow to the hub, blade, and shroud surface of the first and second rotors is shown in Table 3. Because of the lower surface area of the partial shroud, the total heat transfer on the blade is lower in these geometries. In the shroud section, the PS case has a reduction of 33 and 20% compared to the FS case for the first and the second rotors, respectively. The EPS case has a reduction of 29 and 18% on the same location. This value indicates that the heat load reduction is enhanced in the first rotor, where a high aerodynamic loading is higher compared to the second stage and therefore the impact of the shroud geometry on the heat load is higher. The effect of the cooling channel is evident on the suction and pressure sides where the temperature is limited to about 1000 K. At the trailing-edge region, the temperature increases considerably up to 1300 K. This increase is due to the absence of cooling in this region, because the cooling channel is not designed to have any coolant ejection from the blade trailing edge as is common practice in HP turbine blades. For this reason, with the current configuration, the only way to reduce the temperature at the trailing edge is through the internal conduction.

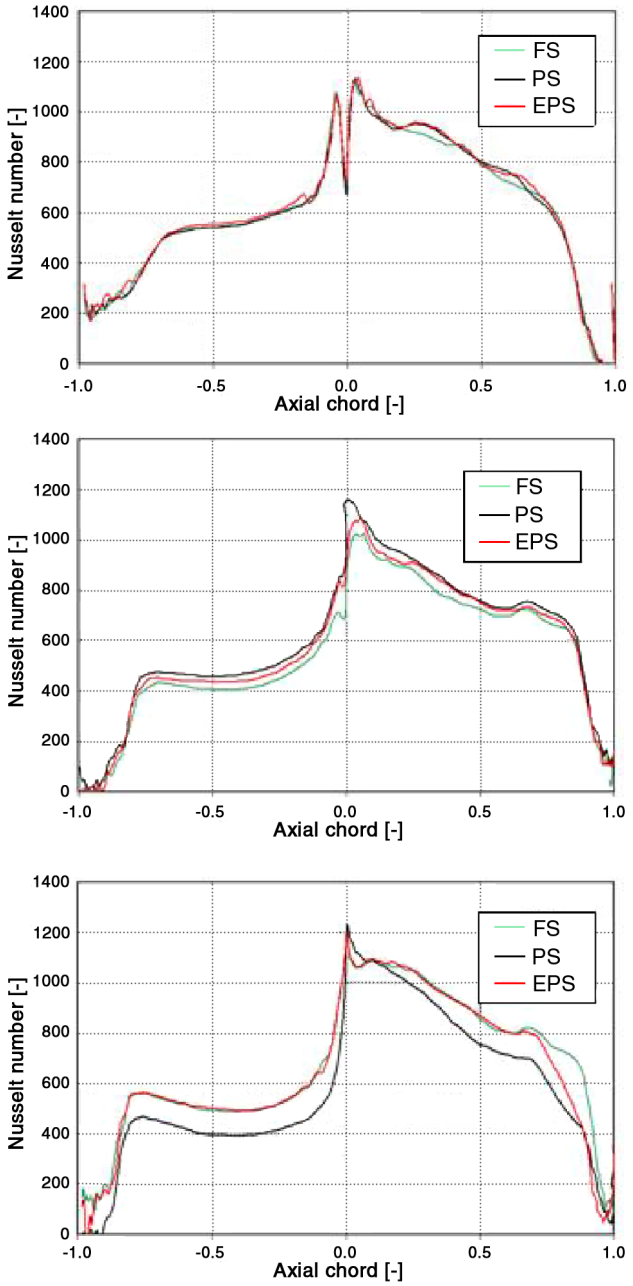

Fig. 5 Calculated Nusselt number distribution at 15% midspan and 85% span on the second rotor surface.

Table 3 Total heat transferred in the hub, blade, and shroud regions in all three test cases in the first and second rotors

	Rotor 1				
	FS, W	PS, W	ΔQ, %	EPS, W	ΔQ, %
Shroud	1754.1	1175.7	−33.0	1240.1	−29.3
Blade	5249.5	5189.5	−1.1	5242.9	−0.1
Hub	646.4	638.9	−1.2	644.4	−0.3
Total	7650.0	7004.0	−8.4	7127.5	−6.8
	Rotor 2				
	FS, W	PS, W	ΔQ, %	EPS, W	ΔQ, %
Shroud	1354.5	1076.6	−20.5	1110.2	−18.0
Blade	4339.0	4267.9	−1.6	4342.0	+0.1
Hub	662.1	666.4	+0.6	666.9	+0.7
Total	6355.6	6010.9	−5.4	6119.1	−3.7

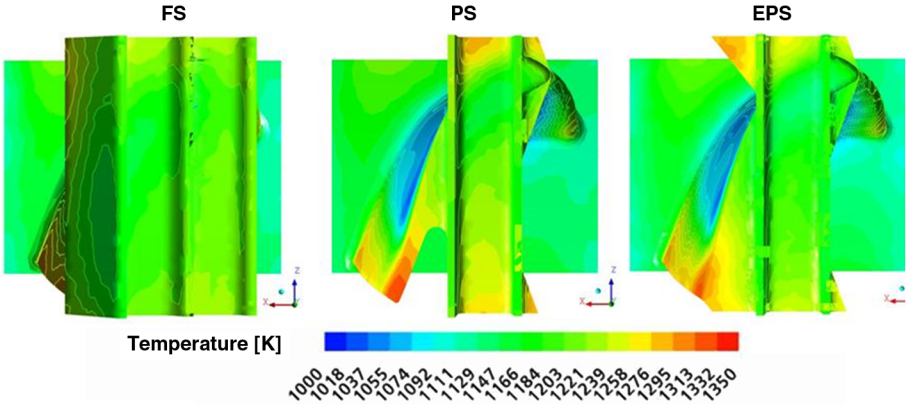

Fig. 6 Calculated temperature distribution on the second rotor surface.

This heat conduction is not sufficient to reduce the blade temperature in this region and the resultant thermal gradient is significant and cannot be sustained during normal operation. However, because the blade geometry and the cooling channel are identical in the three test cases, the results of this analysis can be compared and the effect of the different shroud geometry can be assessed. In the FS case, the blade surface temperature has a lower value, including the trailing-edge region. The conduction effect due to the full shroud decreases the temperature in the blade. In the PS case, the trailing-edge blade tip has the highest temperature due to the absence of the shroud platform, thus no heat is removed through conduction. The EPS case has temperatures intermediate to the other two cases and also very high temperatures along both the trailing-edge section and the shroud platform. Temperature distribution on the shroud upper surfaces is shown. As seen also in Fig. 6, the PS and EPS cases have very high peak temperature at the blade trailing-edge region and, additionally, a higher gradient in the shroud surface. These gradients induce thermal stresses on the material that are quantified in the next sections.

Effect of the Shroud on Mechanical Stress

The effect of the shroud geometry on the mechanical stresses and an estimate of the life of the turbine blade in the simulated flow conditions are addressed. Although demands of increased thermodynamic efficiency have received enormous attention in recent years, there are still many limitations and challenges that designers need to take into account regarding the level of mechanical and thermal stresses that the blades experience. The performance and the durability of gas turbine components are strongly dependent both on the operating conditions and in the environment in which they function. For this reason, much research has focused on the development of advanced materials as nickel-based superalloys. The evolution of directionally solidified and single-crystal alloys has resulted in higher temperature creep and fatigue strength.

Figure 7 shows the predicted equivalent von Mises stresses at the blade surface due to the centrifugal load. The three contour plots have the same scale, thus the test cases can be directly compared. The FS case, with a full shroud configuration and three fins, has a higher mechanical stiffness for bending and torsion. Thus the stresses on the shroud surface have no significant peaks, that is, no stress concentration is observed. The maximum stresses are about 300 MPa which are reasonable values. In the PS and EPS cases, however, the shroud geometry has a lower stiffness and therefore is more sensitive to the centrifugal force that acts on the shroud overhang over the pressure side. For this reason a stress concentration is observed in the shroud fin in both cases. In the EPS case, due to the shroud platform toward the TE, this stress concentration is slightly reduced.

Despite this behavior, the average stresses on the blade surface are significantly lower compared to the FS case. On the pressure side, the FS case has values between 140 and 410 MPa whereas the EPS and PS cases have similar values between 98 and 220 MPa. The resultant reaction force applied on the blade root surface is equal to 68.1 kN in the FS case that corresponds to an average stress of 19.5 MPa. In the PS and EPS cases these values are lower, 15.2% and 14.7%, respectively, as shown in Table 4.

From this analysis it is clear that the FS suffers from a higher weight of the full shroud arrangement and therefore the mechanical stresses due to centrifugal force are, on average, about 15% higher than the partial shroud arrangements. However, due to the less stiff design of the partial shroud cases, the maximum stresses are higher in the PS and EPS cases in the region of the first shroud fin by about 29 and 20%, respectively, compared to the FS case (Table 4). These stress concentrations reduce the blade life, particularly in terms of the maximum number of allowable cycles.

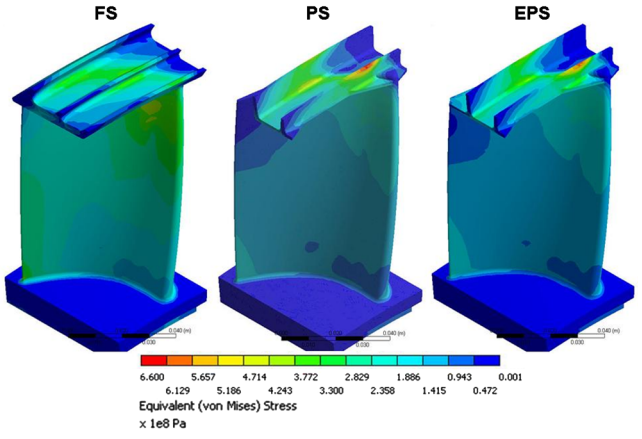

Fig. 7 Calculated von Mises equivalent stresses due to centrifugal load in the second rotor.

Table 4 Total force and mechanical averaged stress at the blade root surface due to centrifugal load

	FS	PS	EPS
Force, N	68,165	57,789	58,119
Stress, MPa	19.45	16.49	16.58
Difference	——	−15.2%	−14.7%
Max stress, MPa	505	652	605
Difference	——	−29.1%	−19.8%

Table 5 Maximum mechanical stresses due to thermal gradient

	FS	PS	EPS
Max stress, MPa	393	513	364
Difference	——	+30.5%	−7.4%

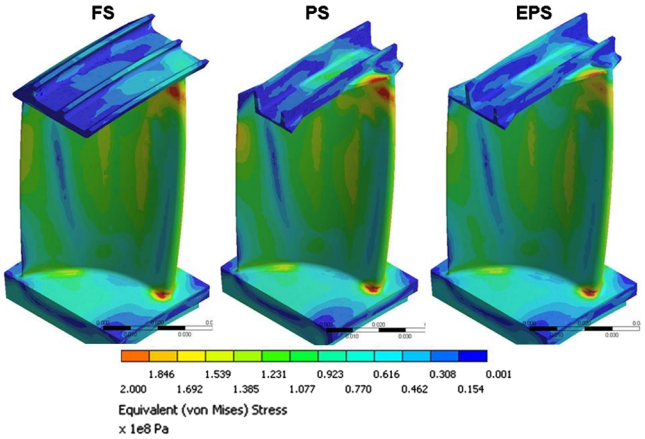

Fig. 8 Von Mises equivalent stresses due to thermal load.

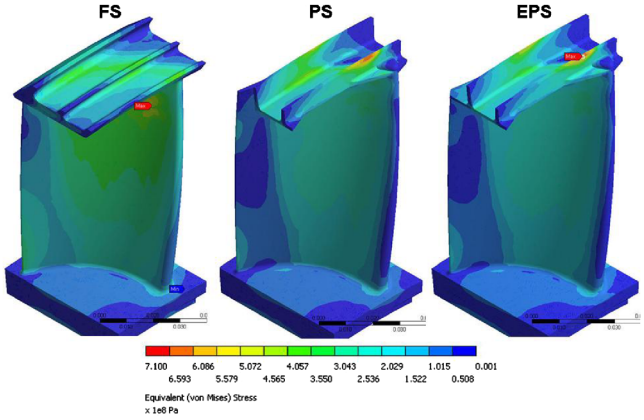

Fig. 9 Total von Mises equivalent stresses due to centrifugal, aerodynamic, and thermal loads.

The mechanical stresses due to thermal loading are shown in Fig. 8 and summarized in Table 5. The boundary conditions for this prediction are identical to the centrifugal load case. The thermal stresses are of the same magnitude but lower than the stresses due to centrifugal force. High values of about 200 MPa are observed in all test cases at the blade leading edge of the hub and tip sections. Additionally on the pressure surface the thermal stress induced by the cooling channel can be seen. In the shroud region, the FS case has the lowest values compared to the PS and EPS cases, which are quite similar.

The main differences between the test cases are observed in the maximum values of the thermal stresses and the location of the stress concentration. In the FS and EPS cases, a stress concentration is located in the cooling channel trailing edge. This stress concentration is attributed to the presence of a notch in this region due to the low radius of curvature. The design of the cooling channel therefore should be modified to decrease this stress concentration. In the PS case the maximum stress is located at the tip at the junction between the shroud and the blade. The magnitude of the stress at this point is about 30% higher compared to the maximum stress in the FS case.

The mechanical stresses due to aerodynamic loading on the blade surfaces are significantly lower compared to the centrifugal and thermal loading. Maximum stresses are about 25 times lower than the stresses due to centrifugal force and for all test cases. The resultant load on the blade root is also approximately 50 times smaller compared to the centrifugal load as shown in Table 6. It is thus concluded that the contribution of the aerodynamic loading on the rotor blade is rather small and can be neglected during the mechanical design phase.

The total stresses resulting from the centrifugal, aerodynamic, and thermal loadings are presented in Fig. 9. The maximum values are close to 700 MPa which is quite close to the yield stress of the material. The combined effect of the different loads on the blades shows that the PS case has the highest stress concentrations due to the low stiffness of the shroud. The maximum stress is 4.3% higher compared to the FS case. The EPS case, however, due to the shroud platform junction with the blade, has a value of the maximum stress that is reduced by 7.5%. The resulting loads on the blade root surface are between 5.9 and 6.9 tons per blade and the PS and EPS cases show a reduction of 14.9 and 14.4%, respectively (Table 7). These numbers provide an indication of the safety factors of these designs and are estimated to be 1.33 for the FS case, 1.27 and 1.43 for the PS and EPS cases, respectively.

Table 6 Total force on the blade root and maximum mechanical stress due to aerodynamic load

	FS	PS	EPS
Max stress, MPa	18.8	20.7	20.3
Difference	——	+10.6%	+8.3%
Force at the root, N	1494	1501	1480
Difference	——	+0.5%	−0.9%

Lifetime Prediction

The life prediction of hot-section components is an important task that every turbine designer is required to assess, because the replacement of these components has a great financial impact. The blade life is mainly influenced by the static and dynamic stress fields on the blade, fatigue properties of the material, loading history, and the environmental operation. Fatigue cracks are usually initiated in a region of stress concentration where some metallurgical discontinuity appears. If critical conditions of operation are sustained, the crack may grow to failure. The life of the blade material is, in addition, very sensitive to the surface blade temperature. It is estimated that at the high temperatures for which the blades are designed in modern gas turbines, an increase of only 20 K at the surface can lead to a reduction of 50% of the blade life. These considerations show that the failure problem is very specific and an accurate prediction of residual blade life is still a challenging task. Moreover, industrial gas turbines operate at different conditions compared to aeroengines and therefore the requirements for the service time and number of cycles may differ considerably.

Several studies have examined blade life prediction. Thulin and Howe [28] reported the design and the life assessment of the NASA E^3 high-pressure turbine. They performed a thermal and mechanical analysis and estimated the life of the rotor blades in 10.000 h corresponding to 2200 flight missions. Dhar et al. [29] performed a transient analysis of the response to the aerodynamic vibratory stress, centrifugal force, and thermal stresses. The latter was achieved by increasing the gas temperature from ambient condition to 840°C and then held constant to simulate a typical startup of a gas turbine. Results show that the centrifugal stresses reach 0.7 of the yield stress of the material and the thermal stresses have a maximum value of 0.55 during the transient startup procedure. According to their cumulative damage analysis, the life of the rotor blade is estimated in about 2100 cycles.

Fatigue Analysis

Blade fatigue can very seriously affect the operation of turbomachinery leading sometimes to catastrophic failures. Because fatigue is always related to a time-dependent load, a lot of effort has been made to assess the natural frequency of vibration and the mode

Table 7 Total force on the blade root and maximum mechanical stress due to centrifugal, aerodynamic, and thermal loads

	FS	PS	EPS
Max stress, MPa	676	705	625.00
Difference	——	+4.3%	−7.5%
Safety factor	1.33	1.27	1.43
Force at the root, N	69,659	59,290	59,599
Difference	——	−14.9%	−14.4%

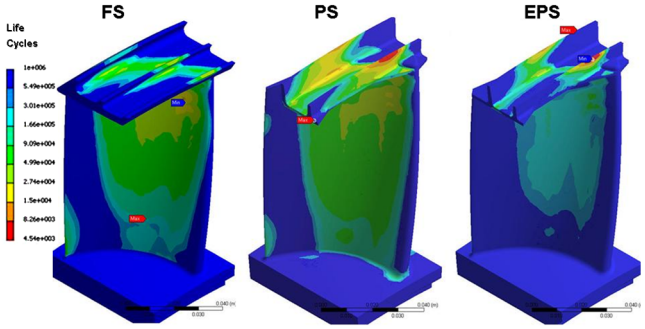

Fig. 10 Maximum number of cycles before rupture due to LCF.

shapes. High-cycle fatigue (HCF) is associated with the application of a large number of low-stress loads and often is caused by vibration, which can directly affect all components. However, generally blades are designed to avoid high-cycle fatigue and thus this failure mode is rare in turbine blades, unless some form of initiating damage is present.

Beside this, during the startup and shutdown of industrial gas turbine or during takeoff and cruise of aeroengines, the blades experience a load that varies from idle (or zero) to maximum. These load variations are associated with the so-called low-cycle fatigue (LCF). For aircraft engines, LCF is the most significant life-reducing failure mechanism and is the result of the many throttle changes experienced during operation (Naeem et al. [30], Salam et al. [31]).

In the present work, a life estimation of the blade of the three test cases has been done using a low-cycle fatigue failure analysis. The loads are varied from zero to maximum values simulating a startup and shutdown procedure that is considered more severe compared to a change of the operating point. The different loads have been varied individually and simultaneously.

The results are shown in Fig. 10 where the maximum number of allowable cycles at different positions in the blade are shown when the total load is varied from 0 to maximum. It is observed that the PS case, as expected from the stress analysis, presents the lowest values on the shroud fin. That means that the number of cycles of the blade is limited to the stress concentration found in that region. In the FS the most critical location is corresponding to the tip section of the cooling channel where thermal gradients and an increase in centrifugal stress are both significant. Table 8 shows the results of the maximum cycle allowed due to each load and due to the sum of all the loads. It is found that the centrifugal load is the most critical due to the higher level of stresses in the blades and it causes the highest level of "damage." The FS case results in a longer life of about 11,000 cycles while the PS and EPS cases have a 50% reduced life. The aerodynamic load does not affect the LCF because the magnitude of this load is 30 times lower than the centrifugal load. The resultant blade life is higher than 10^6 cycles.

If the combination of all three loads is taken into account, it is found that the EPS case has the best performance of 5700 cycles while the FS case lasts for 4700 cycles. The PS case has a quite poor performance and, due to the stress concentrations, is estimated to fail after only 567 cycles which is considered unsatisfactory in an aeroengine application and at the limit for a stationary gas turbine. The lives evaluated from the FS and EPS cases are in the range of other studies (Thulin and Howe [28], Dhar et al. [29]).

Table 8 Maximum number of cycles allowed due to centrifugal, aerodynamic, thermal, and total loads

Loads	FS	PS	EPS
Centrifugal	11,323	5084	6393
Thermal	27,342	10,725	35,999
Aerodynamic	$>10^6$	$>10^6$	$>10^6$
Total	4759	567	5737
Difference	——	−88%	+21%

Creep Analysis

Materials used for elevated temperature service very often experience time-dependant deformation. This leads to a finite lifetime of the components because of limited capability of the materials due to plastic deformation. The ultimate limit is given by fracture, as a result of an increasing accumulation of creep damage. Turbine blades are exposed to high temperature and high mechanical stresses for relatively long periods during operation; therefore creep can be a failure mode. Further complications may arise by high temperature corrosion. The need for an accurate method for predicting creep life during long time operation has resulted in a great number of analytical models and studies that use data extrapolated from accelerated experiments on test specimens including Marahleh et al. [32] and Kablov et al. [33].

In the present analysis, the blade performance in terms of life evaluation is estimated by using the widely accepted technique proposed by Larson-Miller [34]. This method correlates stress, temperature, and rupture life and is defined as

$$\mathrm{LMP} = 1.8T(C + \log t) \cdot 10^{-3}$$

where C is a constant whose values vary between 15 and 25, depending on the alloy and is derived form a least-square fitting of experimental data. A value of $C = 20$ is typically selected for low-alloy steels which yields a conservative estimate of rupture life. For high-performance alloys this parameter can be lower as indicated by some studies (Nicoll [35] and Jaske and Shannon [36]). In the current analysis, the rupture time of 10,000 h has been selected and the LMP constant is 18. The Larson-Miller parameter (LMP) data of the material are taken from Kablov et al. [33] who tested and reported the material properties of the third-generation single-crystal alloy CMSX-10. Figure 11 shows (scattered points) the combination of the total stress and temperature at each point in the solid domain of the blade for 10.000 h of service. The dashed lines represent the Larson-Miller stress-rupture strengths of the CMSX-10 superalloys. All points that lie below the LMP limit of the material are considered safe within the limit of 10.000 h of operation.

The analysis of the LMP in Fig. 11 shows that in all cases, some points exceed the stress-rupture strength of the material, showing that the actual design of the blade cooling system is not sufficient to keep the temperature (and the induced thermal stresses) at an acceptable level in a design life of 10.000 h. In particular, as already seen from the temperature distribution, the blade trailing edge experiences a very high temperature due to the lack of cooling effectiveness and also high thermal and centrifugal stresses. However, still a direct comparison of the test cases can be done based on the relative differences rather than absolute values. The FS and the EPS cases show only very few points above the LMP curve, while the PS case presents a considerable number of points with high stresses and high temperature that exceed the maximum tolerable values. It can be concluded that the PS case has a much lower number of hours of service compared to the FS and EPS cases.

Discussion

The aerothermal comparison of the three test cases has quantified the influence of the shroud geometry on the aerodynamic performance, heat load, and life of the blade component. Table 9 summarizes the main results of this comparative analysis. The FS case with a full axisymmetric shroud is taken as a reference in this discussion.

The flowfield and performance measurements indicate that the PS case has a reduction of 1.1% efficiency on the second stage which is considered significant. It is found that (Porreca et al. [6]) the region where most of the losses are generated is the labyrinth path and the reentry of the leakage flow in the main stream. In this location, an aerodynamic penalty of about 10% of the total stage losses compared to the FS case is observed (15.7% in the FS case compared to 25.8% in the PS case). On the other hand, it has been shown that the modification at the shroud platform on the EPS case is effective. It prevents the flow expansion in the cavity region and the flowfield is

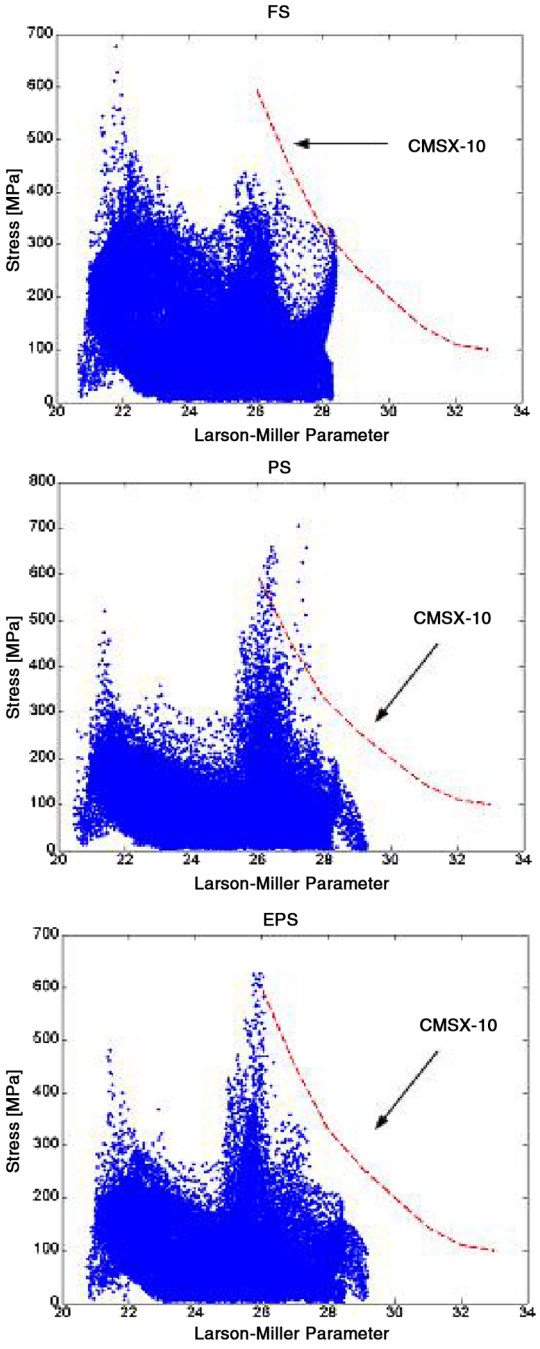

Fig. 11 Larson-Miller parameter for the CMSX-10 superalloy (Kablov et al. [33]) and evaluated in the FS, PS, and EPS test cases.

significantly modified toward the design intent of an axisymmetric full shroud. The EPS second stage aerodynamic efficiency has been improved by about 0.6% compared to the PS partial shroud case. This finding quantifies the aerodynamic benefit of an improved matching between blade and shroud design.

Compared to a full shroud, the partial shroud arrangement has a smaller surface area and therefore the total heat transferred to the blade decreases. Numerical simulations confirm this advantage. By applying the same cooling strategy to all three test cases, it is found that the total heat transferred to the shroud of the second rotor blade is −20 and −18% lower than the full shroud for the PS and EPS cases, respectively. These figures indicate that the coolant flow requirements spilled from the compressor section can be decreased of the same proportion with an advantage in the cycle efficiency of the overall gas turbine installation.

However, it should be stressed that the measurements (Porreca et al. [6]) show a very high level of unsteadiness in the partial shroud case (PS), moderately reduced in the EPS case at the exit of the rotors and close to the tip region. This unsteadiness increases the migration of hot gas from the upstream NGV toward the pressure side and radially upward as it is shown in other studies (Dorney et al. [37]). Additionally, the shroud cutback at the leading edge allows hot gas to penetrate inside the labyrinth path. Therefore, a passive cooling strategy should be adopted to prevent this migration by means of a coolant jet as shown in Janke et al. [13]. Furthermore, the use of small internal cooling passages as in the design proposed by Lilliker et al. [38] and Evans et al. [7] is quite challenging due to the small dimensions of the shroud fins and the nonaxisymmetric geometry. For these reasons even though the coolant mass flow required is lower than in a full shroud arrangement, the cooling strategy is still an open issue and might be a limitation for this geometry.

Table 9 Comparison between aerodynamic performance, heat load, and blade life

	FS	PS	EPS
Aerodynamic efficiency	——	−1.1%	−0.5%
Total heat load, W	6355.6	−5.4%	−3.7%
Blade life			
No. of cycles	4759	−88%	+21%
No. of hours	<10, 000	<2000	<10, 000

The blade life estimation reveals that a stress concentration occurs in both partial shroud cases at the junction between shroud and blade. This phenomenon can be avoided by increasing the fillet radius. Additionally, the shroud structure appears to be unbalanced in the overhang between pressure and suction side of the blade. In some HP turbine blade (Harvey [10]) the shroud is designed to have the same overhang on both blade sides, with the intention to decrease stress concentration. The same design can be applied in the shroud design adopted in the present work and it is believed that the stresses in the PS and EPS cases would be reduced and thus the blade life case would increase considerably compared to the FS case.

However, even with the current design the EPS case has the best life performance (+21% in allowable number of cycles), with a reduction of 3.7% in the heat load and penalty of 0.5% in the aerodynamic efficiency compared to the FS case. Therefore, it can be concluded that the EPS case represents an optimum between the full shroud design and the fully unshrouded configuration.

Conclusions

This study presents a unique experimental and numerical study of three industrially relevant turbine shroud configurations. In the full shroud case the interaction between the leakage flow and the main stream is relatively low compared to the two partial shroud cases where the effect of the leakage flow on the evolution of the secondary flows and associated losses is significant. The measured aerodynamic efficiency penalty of the partial shroud case is 1.1% in comparison with the full shroud case, whereas the enhanced partial shroud geometry reduces the penalty to 0.6%.

The present work quantifies also the impact of the shroud on the heat load and the resultant mechanical stresses. The simulations show that the heat load is reduced in the partial shroud cases due to the reduced area. This may result in lower cooling requirements in terms of coolant mass flow; however, effective internal cooling is challenging due to geometrical limitations and as passive cooling may suffer from the migration of hot gas into the cavity region.

To complete the analysis, blade life estimation has been made based on low-cycle fatigue and creep study. The maximum allowed number of cycles that the blade can sustain is reduced by more than 80% in the partial shroud test case compared to the full shroud case. This behavior is attributed to the stress concentration occurring in the junction between the shroud and the blade in the shroud fin. The enhanced partial shroud case exhibits a superior performance due to a more uniform stress distribution in the shroud resulting to an increase of 20% in the maximum number of cycles over the full shroud case. These features, combined with the reduction of heat load and a

limited aerodynamic efficiency penalty, suggest that this geometry has optimum aerothermal performance despite the small geometrical modification compared to the partial shroud case.

References

[1] Yaras, M. I., and Sjolander, S. A., "Measurements of the Effects of Winglets on Tip-Leakage Losses in a Linear Cascade," ISABE Paper 91-7011, 1991, pp. 127–135, 199.

[2] Harvey, N. W., Willer, L., Newman, D. A., and Haselbach, F., "An Investigation into Novel Turbine Rotor Winglet. Part 1: Design and Model Rig Test Results," American Society of Mechanical Engineers Paper IGTI GT2006-90456, May 2006.

[3] Harvey, N. W., and Ramsden, K., "A Computational Study of a Novel Turbine Rotor Partial Shroud," *Journal of Turbomachinery*, Vol. 123, No. 3, 2001, pp. 534–543. doi:10.1115/1.1370166

[4] Nirmalan, N. V., and Bailey, J. C., "Experimental Investigation of Aerodynamic Losses of Different Shapes of a Shrouded Blade Tip Section," American Society of Mechanical Engineering Paper IGTI GT2005-68903, 2005.

[5] Schabowski, Z., and Hodson, H., "The Reduction of Tip Leakage Loss in Unshrouded Axial Turbines Using Winglets and Squealers," American Society of Mechanical Engineering Paper IGTI GT2007-27623, 2007.

[6] Porreca, L., Kalfas, A. I., and Abhari, R. S., "Optimized Shroud Design for Axial Turbine Aerodynamic Performance," *Journal of Turbomachinery*, Vol. 130, No. 3, July 2008, p. 031016. doi:10.1115/1.2777187

[7] Evans, N. M., Hayton, P., and Hill, S. P., "Gas Turbine Blade Having Improved Thermal Stress Cooling Ducts," U.S. Patent 4560486, 24 Oct. 1995.

[8] Dorris, A. R., North, W. E., and Malandra, A. J., "Gas Turbine Blade Having a Cooled Shroud," U.S. Patent No. 5482435, 9 Jan. 1996.

[9] Tomita, Y., "Gas Turbine Rotor," U.S. Patent No. 5785496, 28 July 1998.

[10] Harvey, N., "Aero-Thermal Implication of Shrouded and Shroudless Blades," *Turbine Blade Tip Design and Tip Clearance*, VKI Lecture Series Vol. 2004-02, 2004.

[11] Nirmalan, N. V., Bailey, J. C., and Braaten, M. E., "Experimental and Computational Investigation of Heat Transfer Effectiveness and Pressure Distribution of a Shrouded Blade Tip Section," American Society of Mechanical Engineering Paper IGTI GT2004-53279, 2004.

[12] Kanjirakkad, T. R., Hodson, H., Janke, E., Haselback, F., and Whitney, C., "Passive Shroud Cooling Concepts of HP Turbines: Experimental Investigations," American Society of Mechanical Engineering Paper IGTI GT2006-91250, 2006.

[13] Janke, E., Haselbach, F., Whitney, C., Kanjirakkad, V., Thomas, R., and Hodson, H., "Passive Shroud Cooling Concepts for HP Turbine: CFD Based Design Approach," American Society of Mechanical Engineering Paper IGTI GT2006-91194, 2006.

[14] Porreca, L., "Aero-Thermal Optimization of Partially Shrouded Axial Turbine," Ph.D. Thesis, Dissertation N. 17138, ETH, Zurich, 2007.

[15] Treiber, M., Kupferschmied, P., and Gyarmathy, G., "Analysis of the Error Propagation Arising from the Measurements with a Miniature Pneumatic 5-Hole Probe," *XIVth Symposium on Measuring Techniques for Transonic and Supersonic Flows in Cascades and Turbomachines*, Limerick, Ireland, 1998.

[16] Bohn, D. E., Becker, V. J., and Kusterer, K. A., "3-D Conjugate Flow and Heat Transfer Calculations of a Film-cooled Turbine Guide Vane at Different Operation Conditions," American Society of Mechanical Engineering Paper IGTI 1997-GT-23, 1997.

[17] Moser, S., Ivanisin, M., Woisetscgläger, J., and Jericha, H., "Novel Blade Cooling Engineering Solution," American Society of Mechanical Engineering Paper IGTI 2000-GT-242, 2000.

[18] Takashashi, T., and Watanabe, K., "Thermal Conjugate Analysis of a First Stage Blade in a Gas Turbine," American Society of Mechanical Engineering Paper IGTI 2000-GT-251, 2000.

[19] Wright, L. M., Fu, W. L., and Han, J. C., "Thermal Performance of Angled, V-Shaped, and W-Shaped Rib Turbulators in Rotating Rectangular Cooling Channels (AR = 4:1)," *Journal of Turbomachinery*, Vol. 126, No. 4, Oct 2004, pp. 604–615. doi:10.1115/1.1791286

[20] Griffith, T. S., Hadhrami, A. L., and Han, J. C., "Heat Transfer in Rotating Rectangular Cooling Channels (AR = 4) with Dimples," *Journal of Turbomachinery*, Vol. 125, No. 3, 2003, pp. 555–564. doi:10.1115/1.1571850

[21] Han, B., and Goldstein, R. J., "Jet-Impingement Heat Transfer in Gas Turbine Systems," *Annals of the New York Academy of Sciences*, Vol. 934, 2001, pp. 147–161.

[22] Brevet, P., Dorignac, E., and Vullierme, J. J., "Mach Number Effect on Jet Impingement Heat Transfer," *Annals of the New York Academy of Sciences*, Vol. 934, No. 1, 2001, pp. 409–416.

[23] Son, C., Gillespie, D., and Ireland, P., "Heat Transfer and Flow Characteristics of an Engine Representative Impingement Cooling System," American Society of Mechanical Engineering Paper IGTI 2000-GT-219, 2000.

[24] Berruti, T., Filippi, S., Goglio, L., Gola, M. M., and Salvano, S., "A Test Rig for Frictional Damped Bladed Segments," *Journal of Engineering for Gas Turbines and Power*, Vol. 124, No. 2, April 2002, pp. 388–394. doi:10.1115/1.1419015

[25] Griffin, J. H., "Friction Damping of Resonant Stresses in Gas Turbine Engine Airfoils," *Journal of Engineering for Power*, Vol. 102, No. 2, 1980, pp. 329–333.

[26] Berthillier, M., Dupont, C., Mondal, R., and Barrau, J. J., "Bladed Force Response—Analysis with Friction Dampers," *Journal of Vibration and Acoustics*, Vol. 120, No. 2, 1998, pp. 468–474. doi:10.1115/1.2893853

[27] Herron, W. L., "Turbine Bucket Tip Shroud Reinforcement," U.S. Patent 6241471 issued on 5 June 2001.

[28] Thulin, R. D., and Howe, C. D., "Energy Efficient Engine—High Pressure Turbine Detailed Design Report," NASA CR-165608, 1982.

[29] Dhar, D., Sharan, A. M., and Rao, J. S., "Transient Stress Analysis and Fatigue Life Estimation of Turbine Blades," *Journal of Vibration and Acoustics*, Vol. 126, No. 4, Oct. 2004, pp. 485–496. doi:10.1115/1.1804996

[30] Naeem, M., Singh, R., and Probert, D., "Implications of Engine Deterioration for High-Pressure Turbine-Blade's Low Cycle Fatigue (LCF) Life-Consumption," *International Journal of Fatigue*, Vol. 22, No. 2, Feb. 2000, pp. 147–160. doi:10.1016/S0142-1123(99)00105-X

[31] Salam, I., Taquir, A., and Khan, A. Q., "Creep-Fatigue Failure of an Aero Engine Turbine Blades," *Engineering Failure Analysis*, Vol. 9, No. 3, June 2002, pp. 335–347. doi:10.1016/S1350-6307(01)00011-5

[32] Marahleh, G., Kheder, R. I., and Hamad, H. F., "Creep Life Prediction of Service-Exposed Turbine Blades," *Materials Science and Engineering A*, Vol. 433, No. 1, Oct. 2006, pp. 305–309. doi:10.1016/j.msea.2006.06.066

[33] Kablov, E. N., Toloraiya, V. N., and Orekhov, N. G., "Single Crystal Rhenium-Bearing Nickel Alloys for Turbine Blade of GTE," *Metal Science and Heat Treatment*, Vol. 44, Nos. 7–8, July 2002.

[34] Davis, J. R., *Materials Handbook*, 10th ed., ASM International, Materials Park, OH, 1992.

[35] Nicoll, R., "The Larson-Miller Constant Applied to a Cobalt-Based Directionally Solidified Eutectic Alloy," *Journal of Material Science and Technology (Sofia)*, Vol. 14, No. 7, 1979, pp. 1759–1761.

[36] Jaske, C. E., and Shannon, B. E., "Inspection and Remaining Life Evaluation of Process Plant Equipment," *Proceedings of the Process & Power Plant Reliability Conference, Houston*, 13–14 Nov. 2002.

[37] Dorney, D. J., Davis, R. L., Edwards, D. E., and Madavan, N. K., "Unsteady Analysis of Hot Streak Migration in a Turbine Stage," *Journal of Propulsion and Power*, Vol. 8, No. 2, 1992, pp. 520–529. doi:10.2514/3.23507

[38] Lilliker, J. R., Henshaw, H., Winter, J. I., "Cooling of Turbine Blades," U.S. Patent 4940388, 10 July 1990.

F. Liu
Associate Editor